

Candidate Population III stellar complex at $z=6.629$ in the MUSE Deep Lensed Field

E. Vanzella^{1*}, M. Meneghetti¹, G. B. Caminha², M. Castellano³, F. Calura¹, P. Rosati^{4,1}, C. Grillo⁵, M. Dijkstra, M. Gronke⁶, E. Sani⁷, A. Mercurio⁸, P. Tozzi⁹, M. Nonino¹⁰, S. Cristiani¹⁰, M. Mignoli¹, L. Pentericci³, R. Gilli¹, T. Treu¹¹, K. Caputi², G. Cupani¹⁰, A. Fontana³, A. Grazian¹² and I. Balestra^{10,13}

¹INAF – Osservatorio di Astrofisica e Scienza dello Spazio, via Gobetti 93/3, 40129 Bologna, Italy

²Kapteyn Astronomical Institute, University of Groningen, Postbus 800, 9700 AV Groningen, The Netherlands

³INAF – Osservatorio Astronomico di Roma, Via Frascati 33, I-00078 Monte Porzio Catone (RM), Italy

⁴Dipartimento di Fisica e Scienze della Terra, Università degli Studi di Ferrara, via Saragat 1, I-44122 Ferrara, Italy

⁵Dipartimento di Fisica, Università degli Studi di Milano, via Celoria 16, I-20133 Milano, Italy

⁶Department of Physics, University of California, Santa Barbara, CA 93106, USA

⁷European Southern Observatory, Alonso de Cordova 3107, Casilla 19, Santiago 19001, Chile

⁸INAF – Osservatorio Astronomico di Capodimonte, Via Moiariello 16, I-80131 Napoli, Italy

⁹INAF – Osservatorio Astrofisico di Arcetri, Largo E. Fermi, I-50125, Firenze, Italy

¹⁰INAF – Osservatorio Astronomico di Trieste, via G. B. Tiepolo 11, I-34143, Trieste, Italy

¹¹Department of Physics and Astronomy, University of California, Los Angeles, CA 90095, USA

¹²INAF – Osservatorio Astronomico di Padova, Vicolo Osservatorio 5, 35122, Padova, Italy

¹³OmegaLambdaTec GmbH, Lichtenbergstrasse 8, 85748 Garching bei Munchen, Germany

ABSTRACT

We discovered a strongly lensed ($\mu \gtrsim 40$) Ly α emission at $z=6.629$ ($S/N \simeq 18$) in the MUSE Deep Lensed Field (MDLF) targeting the Hubble Frontier Field galaxy cluster MACS J0416. Dedicated lensing simulations imply that the Ly α emitting region necessarily crosses the caustic. The arc-like shape of the Ly α extends $3''$ on the observed plane and is the result of two merged multiple images, each one with a de-lensed Ly α luminosity $L \lesssim 2.8 \times 10^{40}$ erg s⁻¹ arising from a confined region ($\lesssim 150$ pc effective radius). A spatially unresolved HST counterpart is barely detected at $S/N \simeq 2$ after stacking the near-infrared bands, corresponding to an observed (intrinsic) magnitude $m_{1500} \gtrsim 30.8$ ($\gtrsim 35.0$). The inferred rest-frame Ly α equivalent width is $EW_0 > 1120 \text{ \AA}$ if the IGM transmission is $T_{\text{IGM}} < 0.5$. The low luminosities and the extremely large Ly α EW_0 match the case of a Population III star complex made of several dozens stars ($\sim 10^4 M_\odot$) which irradiate a HII region crossing the caustic. While the Ly α and stellar continuum are among the faintest ever observed at this redshift, the continuum and the Ly α emissions could be affected by differential magnification, possibly biasing the EW_0 estimate. The aforementioned tentative HST detection tend to favour a large EW_0 , making such a faint Pop III candidate a key target for the James Webb Space Telescope and Extremely Large Telescopes.

Key words: galaxies: formation – galaxies: starburst – gravitational lensing: strong

1 INTRODUCTION

Finding and characterising the first galaxies is the next frontier in observational astronomy. It is thought that the Universe was initially metal-enriched by the first generation of Population III (Pop III) stars, that could also have played

a key role in cosmic reionisation before the formation of primeval galaxies (e.g., Zackrisson, & Vikaeus 2019; Wise 2019; Dayal, & Ferrara 2018, and references therein). Late ($z < 7$) Pop III star formation might also have occurred in pristine regions due to inhomogeneous metal enrichment of the first galaxies (Tornatore, Ferrara & Schneider 2007; Visbal et al. 2016; Salvaterra et al. 2011). Given the exceptionally high effective temperatures of Pop III stars in

* E-mail: eros.vanzella@inaf.it

the zero-age main sequence, they emit a large fraction of their luminosity in the Lyman continuum and have a much harder ionising spectrum than stars with higher metallicity. The main characteristics of their predicted spectral energy distribution (SED) are the presence of a prominent rest-frame Ly α (Lyman-alpha) emission line due to the strong ionising flux up to $\sim 1000 - 4000\text{\AA}$ rest-frame equivalent width (denoted as EW_0 , hereafter) and significant He recombination line (especially HeII $\lambda 1640$, with EW_0 up to $15-40\text{\AA}$) due to spectral hardness, while a clear deficit of all the metal lines is expected. In particular, Inoue (2011) suggested the following criteria for the identification of extremely metal poor or Pop III galaxies: $EW_0(\text{Ly}\alpha) > 230\text{\AA}$, $EW_0([\text{OIII}]\lambda 5007) < 20\text{\AA}$ and $EW_0(\text{HeII}\lambda 1640) > 1\text{\AA}$, and prominent Balmer lines like $EW_0(\text{H}\alpha) > 1900\text{\AA}$, while showing an extremely blue ultraviolet spectral slope ($\beta \sim -3$, $F(\lambda) \sim \lambda^\beta$).

Observations have yielded candidates for Pop III stellar populations at high redshift (e.g., Kashikawa et al. 2012; Sobral et al. 2015, and references therein), yet without any definitive detection. These include a controversial $z = 6.6$ galaxy dubbed CR7 that displays HeII $\lambda 1640$ emission (Sobral et al. 2019; Shibuya et al. 2018). Thus, to date, there has not been a confirmed observation of a galaxy dominated by the flux of Pop III stars. The possibility of observing signatures from very metal poor or Pop III star clusters through gravitational lensing has also been discussed, e.g., Zackrisson et al. (2015) (see also Hernán-Caballero et al. 2017), including the detection of single Pop III stars with fluxes temporarily magnified to extreme values (with the magnification parameter $\mu \simeq 10^3 - 10^5$) during their transit across the caustic of a galaxy cluster. Such single-star-transit events can boost the flux of the star by 7 – 12 mag (Windhorst et al. 2018), making such objects visible for a limited amount of time even down to intrinsic magnitudes of 35 – 38. Examples of such events detecting single normal stars at $z < 2$ have been reported recently by Rodney et al. (2018).

Very low-luminosity emission line galaxies have been identified in Hubble Ultra Deep Field, down to magnitude 30 – 32 ($M_{1500} = -15$) and $S/N \sim 1 - 5$ (Maseda et al. 2018). Strong gravitational lensing allowed us to shed further light on similar low-luminosity objects, providing higher $S/N \sim 20$ for individual cases (e.g., Vanzella et al. 2017, 2019). In this letter we present an object at $z=6.629$ showing (1) the faintest Ly α emission ever detected at $z > 6$ crossing the caustic of the Hubble Frontier Field (HFF) galaxy cluster MACS J0416 (Lotz et al. 2017) and (2) a large Ly α EW_0 , potentially implying that extreme stellar populations are present. We assume a flat cosmology with $\Omega_M = 0.3$, $\Omega_\Lambda = 0.7$ and $H_0 = 70 \text{ km s}^{-1} \text{ Mpc}^{-1}$.

2 THE MUSE DEEP LENSED FIELD: MDLF

VLT/MUSE (Bacon et al. 2010) deep spectroscopic observations of 17.1 hours of integration time in a single pointing have been obtained on the HFF galaxy cluster MACS J0416 (Prog. 0100.A-0763(A), PI Vanzella). The data reduction follows the technique described in Caminha et al. (2017), eventually achieving a PSF with FWHM of $0.6''$ in the final datacube. A more detailed description of the observational campaign of the MDLF and of the data reduction will be presented elsewhere. A refined lens model of HFF J0416 us-

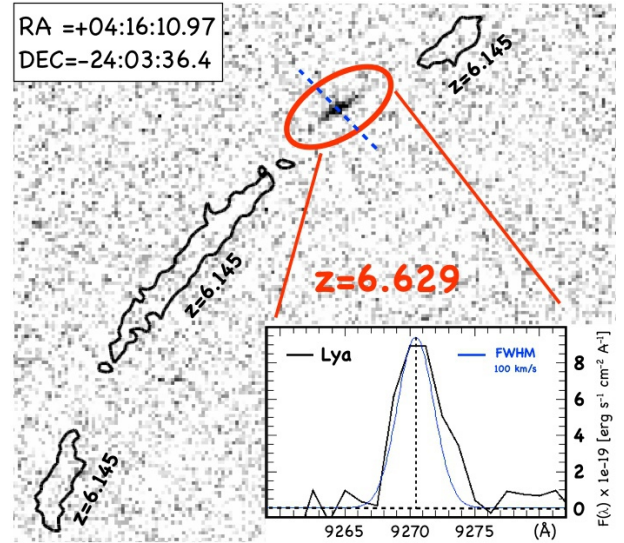


Figure 1. A $30'' \times 30''$ region extracted from the MDLF at the $z=6.629$ Ly α wavelength and averaged over $dv = 200 \text{ km s}^{-1}$. The indicated Ly α arclet straddles the critical line (marked with the blue dotted line), close to a highly magnified system already confirmed at $z=6.145$ and well constrained by the three giant Ly α arcs (black contours). The one-dimensional spectrum of the Ly α line at $z=6.629$ is shown in the inset, where the asymmetry towards the red side is evident (a Gaussian with $\text{FWHM}=100 \text{ km s}^{-1}$ is superimposed with a blue line).

ing a new set of confirmed multiple images from the MDLF, will also be presented in a forthcoming paper.

2.1 A Ly α arc at $z=6.629$ and the faint HST counterpart

Figure 1 shows the extended ($3''$) arc from the continuum subtracted narrow band image extracted from the MUSE data cube and the one-dimensional profile of the emission line at $\lambda = 9270.7\text{\AA}$, in a region free from OH sky emission lines. The arc is detected at $S/N=18$ with flux $4.4 \times 10^{-18} \text{ erg s}^{-1} \text{ cm}^{-2}$ calculated within an elliptical aperture with major and minor axes of $4''$ and $1.5''$, respectively, and shows an asymmetric profile having an instrumental corrected FWHM of $98(\pm 7) \text{ km s}^{-1}$. We identify this line as Ly α at $z = 6.629$ for the following reasons: (1) the weighted skewness S_W (as defined by Shimasaku et al. 2006) is 3.4 ± 0.7 , in line with the typical values observed for asymmetric Ly α emissions at high- z (it is zero for symmetric shapes, Figure 1); (2) if it is identified to other typical lines like $[\text{OII}]\lambda 3727, 3729$, $[\text{OII}]\lambda 4959$, $[\text{OII}]\lambda 5007$, $\text{H}\beta$, or $\text{H}\alpha$, each of them would imply the presence and detection of additional lines in the same spectrum; (3) the MUSE spectral resolution at $\lambda > 9000\text{\AA}$ is $R \simeq 3500$, high enough to resolve the single components of the doublets like $\text{CIV}\lambda 1548, 1550$, $[\text{OII}]\lambda 1661, 1666$, $\text{CIII}\lambda 1907, 1909$, $[\text{OII}]\lambda 3727, 3729$ further excluding these lines for identification. As Figure 2 shows, there is no clear detection in the F105W (Y), F125W (J), F140W (JH), and F160W (H) bands in the HFF images, probing the ultraviolet stellar continuum down to the nominal depth of the HFFs (mag $\simeq 29$, at 5σ limit Lotz et al. 2017). We therefore computed the Y+J+JH+H weighted-mean stacked images

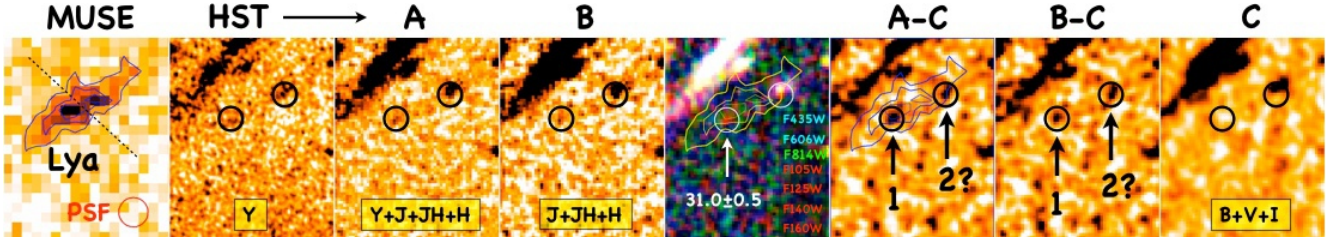


Figure 2. From left to right: the MUSE Ly α emission averaged over $dv = 160 \text{ km s}^{-1}$ (the 2 and 4 σ contours are shown, with the dotted line marking the critical line); the Y-band HST image; the stacked Y+J+JH+H and J+JH+H images with indicated the positions of the two possible high- z counterparts (solid circles with diameter $0.4''$); the colour stacked image; the differential stacked HST images highlighting the two possible counterparts (A-C) and (B-C) after a Gaussian smoothing with $\sigma=1$ pix; the B+V+I stacked image (C).

(probing $\lambda \sim 1500\text{\AA}$), reaching a 1σ limit of 31.6 within circular apertures of diameter $0.4''$. Such a limit has been derived by inserting 30 apertures in free regions surrounding the source position and computing the standard deviation among them (the A-PHOT tool has been used for this task, Merlin et al. 2019). As discussed in the next section, there is a configuration in which we expect the presence of two very close multiple images near the Ly α arc. Indeed, there is a possible detection at $S/N \sim 2$ lying within the arclet indicated as 1 in Figure 2, with $m_{1500} \simeq 31$ and showing a photometric drop in the F435W+F606W+F814W image. The same test has been performed adopting an elliptical aperture oriented along the arc, with semi-axis $0.7''$ and $0.2''$, and no signal has been detected down to $m_{1500} \simeq 30.85$ at 1σ . We expect a second nearby image with similar magnification that, however, is contaminated by a foreground object clearly detected in the blue bands. While image 1 could be the HST counterpart, a tentative second image detection marked as 2 is shown in Figure 2.

3 THE Ly α EMISSION IS ON THE CAUSTIC

The Ly α arc lies in a well known region of the galaxy cluster where Vanzella et al. (2017, 2019) already discussed another star-forming complex system at $z=6.145$ showing several multiple images identified in deep HST data, producing three clear Ly α arcs in the MUSE observations (Figure 1). The presence of such a system adds valuable constraints for the case studied in this work. In fact, any detection at $z > 6$ in the region where the $z=6.629$ arc lies, would produce multiple images as in the case observed at $z=6.145$, unless such images are so close to merge into a single spatially unresolved mildly elongated arc. It is exactly the case for the $z=6.629$ arclet discussed here: the absence of two distinct images (Figure 1 and 2) implies that the Ly α arc straddles the critical line and is indeed the result of two spatially unresolved Ly α images, generated by a Ly α emitting region lying on the corresponding caustic.

3.1 Simulating the caustic crossing

In order to perform a quantitative estimate of the magnification of the Ly α emission, we use dedicated simulations with a customised version of the software SkyLens (e.g. Meneghetti et al. 2010; Plazas et al. 2019). The method will be extensively described in a future paper. In short, we perform the following steps. We start from the assumption that the

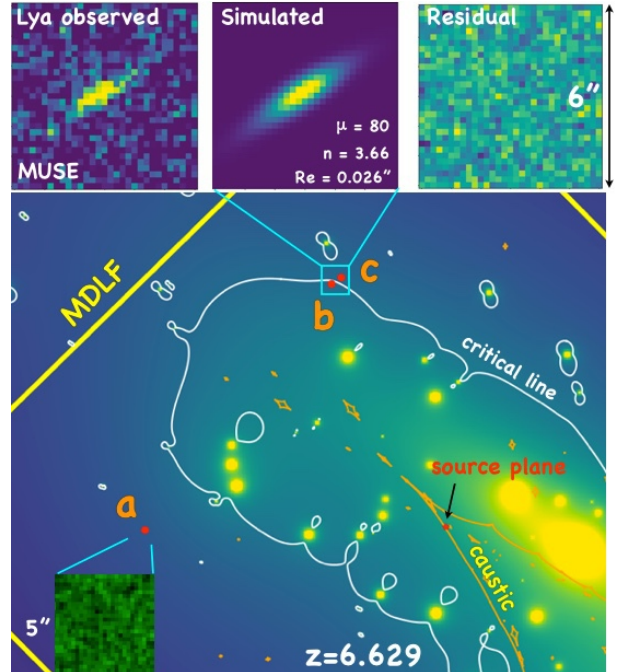


Figure 3. The tangential caustic (orange) and the critical line (white) are superimposed to the (false-colour) image of the galaxy cluster members used for the strong lensing model. The observed Ly α arc is well reproduced when the source is very close to the caustic (black arrow). Three multiple images are predicted (marked as a, b and c): images b,c merge into a single small arc, whereas image a is not detected (bottom-left inset). In the top panels, the observed, simulated and residuals Ly α images are shown for the best fit values of n , R_e and $\mu = \mu(a) + \mu(b)$.

source of the Ly α emission can be described by a single, circularly symmetric Sérsic surface brightness profile. The profile is characterised by the Sérsic index n and by the effective radius R_e . We ray-trace 2000×2000 light rays through a squared region containing the Ly α emission (cyan square in Figure 3, whose size is $\sim 6.2'' \times 6.2''$) and propagate them towards the source plane at redshift $z_s = 6.629$, accounting for the deflections induced by the lensing cluster. In this work, we use the strong lensing model described in Caminha et al. (2017)¹. On the source plane, the arrival

¹ The LensTool model is published in the HFF lens model format at <http://www.fe.infn.it/astro/lensing/>

positions of the light rays are used to sample the brightness distribution of the source, which is then mapped onto the image plane. By performing this operation, we reconstruct the lensed image, which is subsequently convolved with a Gaussian PSF with a FWHM of $0.6''$. The resulting convolved image is first rebinned at the same resolution of the MUSE image ($0.2''/\text{pixel}$) and then compared to the observed Ly α arclet. We use the python package `LMfit` to perform a Non-linear Least Square Minimisation of a cost function defined as the squared difference between the simulated and the observed images. As shown in the upper panels of Figure 3, the source model, despite its simplicity, reproduces very well the observed arclet morphology. The two parameters n and R_e are quite degenerate. For a Sérsic index in the range $n = 1 - 4$, the best fit effective radius R_e varies between $0.012'' - 0.027''$. The best fit solution corresponds to $n = 3.66$ and $R_e = 0.026''$. The latest is equivalent to 140 pc on the source plane. In all cases, the model suggests that the Ly α emitting region partially overlaps with the caustic, meaning that only part of the source is reproduced twice in the arclet.

Having obtained a model for the Ly α source, we can estimate the magnification of the arclet by comparing the lensed and the intrinsic fluxes of the source after integrating the surface brightness over the region used for ray-tracing. We estimate that the total magnification of the Ly α arclet (images b and c) is $\mu(b+c) = \mu(b) + \mu(c) \simeq 80$, implying that the de-lensed Ly α flux of the arclet is $\sim 5.5 \times 10^{-20} \text{ erg s}^{-1} \text{ cm}^{-2}$. Keeping $n \sim 1$ (exponential profile) in our fitting procedure the magnification increases to $\mu(b+c) \sim 110$.

It is well known that such magnification estimate is prone to systematic errors due to the uncertainties of the lens model in regions where the magnification gradients are very strong (e.g., Meneghetti et al. 2017). In order to circumvent this limitation, we can make use of the counter image a, which is predicted to form much farther from the critical lines (Figure 3). Using our best fit source determined above, we estimate that $\mu(a) \sim 4.5$ with an uncertainty smaller than 20%. We also find that, because of the much shallower magnification gradient in this region, the estimate is quite insensitive to the properties of the source. Indeed, $\mu(a)$ would change by $\sim 5\%$ ($\mu(a) \sim 4.3$) by adopting a point source approximation. The image a is not detected at the depth of the MDLF down to 1σ Ly α flux limit $f_{a,lim}$ ($\sim 2.4 \times 10^{-19} \text{ erg s}^{-1} \text{ cm}^{-2}$, for a point-like source, consistently to Inami et al. 2017). This sets a lower limit $\mu(b+c) \gtrsim \mu(a) f_{bc}/f_{a,lim}$, where the observed ratio is $f_{bc}/f_{a,lim} \simeq 18$. Therefore, we can conclude that $\mu(b+c) \gtrsim 80$, in keeping with the fitting procedure ($\mu = 80 - 110$).

3.2 A large Ly α EW

The computation of the EW of the Ly α line (L) requires an estimate of the underlying stellar continuum (S), taking into account that magnifications associated to S (μ_S) and L (μ_L) might differ. A general expression for EW_0 is:

$$EW_0 = \frac{1}{(1+z)} \frac{\mu_S}{\mu_L} \frac{f(\text{Ly}\alpha)}{F_\lambda(\text{UV}) \times T_{\text{IGM}}(\text{Ly}\alpha)}, \quad (1)$$

where $f(\text{Ly}\alpha)$ is the Ly α flux ($5.5 \times 10^{-20} \text{ erg s}^{-1} \text{ cm}^{-2}$), $F_\lambda(\text{UV})$ is the ultraviolet continuum at the Ly α wavelength for which we assume a value $< 1.27 \times 10^{-23} \text{ erg s}^{-1} \text{ cm}^{-2} \text{ \AA}^{-1}$, corresponding to $m_{1500} \gtrsim 35$ (=

$31+2.5\text{Log}_{10}(\mu)$, $\mu \gtrsim 40$). Given the large uncertainties on the HST detection ($S/N \sim 2$, $\sigma_m \sim 0.5$), any assumption on the ultraviolet slope β would not be significant. Indeed, a slope $\beta = -2.5$ (-3) would imply a magnitude difference of $m_{1216} - m_{1500} = -0.11$ (-0.23). $T_{\text{IGM}}(\text{Ly}\alpha)$ is the transmission of the intergalactic medium for Ly α photons (see below, and Table 1). We identify two scenarios:

- if we assume that L and S have the same intrinsic size and brightness profile, then $\mu_S \simeq \mu_L$ and the EW_0 is independent on the lens model. Thus, under this assumption, a lower limit on EW_0 can be found by using the very low significance detection (if not the non-detection) of the UV continuum, $m_{1500} \gtrsim 35$. Combined with the de-lensed Ly α flux of $5.5 \times 10^{-20} \text{ erg s}^{-1} \text{ cm}^{-2}$ leads to the result that $EW_0 > 564 \text{ \AA}$, in the case $T_{\text{IGM}}(\text{Ly}\alpha)=1.0$. The low significance of the HST detection prevents us from verifying whether S is extended as the arclet.
- if, in contrast, we assume that the size of S is smaller than that of L , as it might be the case when S is embedded and generates the HII region (e.g., Steidel et al. 2011), then we expect that $\mu_S > \mu_L$ and consequently EW_0 would be even larger than in the previous case.

There is still the possibility that S is located outside the lens caustic. In this scenario no continuum flux is expected near the Ly α arclet. We could only use the non-detection in the HST data of image a ($m > 31.6$ at 1σ), where S is certainly present, to set an upper limit of $F_\lambda(\text{UV})$. Using the fact that $\mu(a) \sim 4.5$, the de-lensed magnitude limit is $m > 33.2$. Combined with the lower limit of the magnification of L ($\mu_L \gtrsim 80$), we obtain that $EW_0 \gtrsim 110 \text{ \AA}$ in the case $T_{\text{IGM}}(\text{Ly}\alpha)=1.0$. Note, however, that the marginal detection of image 1 in the stacked HST images (see Figure 2), which could be the image of S , seems to disfavour this scenario.

It is now worth discussing the IGM transmission $T_{\text{IGM}}(\text{Ly}\alpha)$ which depends on *both* the ‘‘intrinsic’’ (pre-IGM) Ly α spectrum emerging *and* the IGM properties. Due to the resonant absorption of the neutral or partially neutral IGM combined with cosmological inflow, the Ly α spectrum blueward of $v_{\text{cutoff}} \lesssim 200 \text{ km s}^{-1}$ is absorbed (Dijkstra, & Wyithe 2007). Thus, the more asymmetric the intrinsic Ly α is towards the blue or the lower the red peak offset from systemic, the lower T_{IGM} . All this implies that T_{IGM} is highly uncertain and estimates reach from tens of percent (e.g., $T_{\text{IGM}} = 0.20^{+0.12}_{-0.15}$ at $z = 6.6$, Laursen et al. 2011) to values approaching unity for an intrinsic single read peak with offset $> 300 \text{ km s}^{-1}$. However, since the Ly α spectrum presented here is very narrow and asymmetric (cf. Sect. 2.1) it is likely that either a significant part of the red peak has been removed from the IGM (in case of an intrinsic spectrum with a large offset, and thus, large width), or an intrinsic blue component existed (in the case of a small intrinsic offset). Both cases would imply a significant absorption of the IGM, and hence, $T_{\text{IGM}} < 1$. Knowledge of the systemic redshift, through, e.g., H α information would be helpful in reconstructing the intrinsic Ly α line, and thus, to constrain T_{IGM} more qualitatively. This could, furthermore, rule out the radiative transfer effects as an origin of the large EW – which we already deem unlikely due to the asymmetry of the observed line.

We conclude that, even assuming $T_{\text{IGM}}(\text{Ly}\alpha)=1$, a still quite extreme $EW_0(\text{Ly}\alpha) > 550 \text{ \AA}$ emerges from a region crossing the caustic, that can easily approach (or exceed)

Table 1. Properties of the Ly α emitter in the source plane.

Ly α [erg s $^{-1}$ cm $^{-2}$]	5.5×10^{-20}
Ly α [erg s $^{-1}$]	2.8×10^{40}
EW $_0$ (Ly α) [Å] (T $_{\text{IGM}} < 0.5$)	> 1120
M $_{1500}$ (m_{1500}) (2σ)	$\gtrsim -11.9$ ($\gtrsim 35$)
R_e Ly α region [pc]	< 150
Magnification [$\mu(b) = \mu(c)$]	$\mu(b) + \mu(c) \gtrsim 80$; $\mu(a) \simeq 4.5$

1000Å assuming a more plausible T $_{\text{IGM}}(\text{Ly}\alpha) < 1.0$. Though not totally excluded, we do not consider in this work the possibilities that the large EW(Ly α) originates from a very faint AGN (e.g., with BH mass of $10^{2-3} M_{\odot}$, Fan 2012) or a multiphase scattering medium (e.g., Neufeld 1991).

4 CANDIDATE POP III STARS

The predicted EW $_0$ (Ly α) for metal free stellar populations exceeds 400Å and it goes up to a few thousands rest-frame (Inoue 2011; Schaerer 2013), and is observable if neighbouring sources (either Pop III or Pop II stars) have already contributed toward ionising a local bubble (Sobral et al. 2015). The large EW $_0$ (Ly α) value reported in this work opens for a possible dominant contribution by extremely metal poor stars. It is interesting to calculate how many Pop III stars are needed to reproduce both the observed M $_{1500}$ and L(Ly α):

- *UV continuum*: the apparent magnitudes at 1500Å rest-frame at $z = 7$ for Pop III star at ZAMS with masses 1–1000 M_{\odot} are reported by Windhorst et al. (2018). In particular, stars with masses of 100, 300, and 1000 M_{\odot} have magnitudes $m_{1500} = 40.08, 38.64,$ and 37.44 , respectively, neglecting dust attenuation. Adopting $m_{1500} \gtrsim 35$ ($M_{\text{UV}} \gtrsim -11.9$, Sect. 3.2) and assuming for simplicity the same masses for all stars, the number of Pop III stars required to reproduce the intrinsic UV flux corresponding to M_{UV} amounts to $N(M_{\text{UV}}) = 10, 30,$ and 110 for stellar masses of 1000, 300 and 100 M_{\odot} .
- *Ly α emission*: Mas-Ribas et al. (2016) provide the photon flux $Q(\text{H}\text{I})[\text{s}^{-1}]$ for different Pop III ZAMS stars and the conversion to L(Ly α) luminosity considering case-B departure, stochastic sampling of the Salpeter and Top-Heavy IMF's and zero escape fraction of the Lyman continuum radiation (note, however, that if a fraction of the ionising radiation escapes, the emerging Ly α would be dimmed linearly by the same factor, e.g., Schaerer 2013). We perform the calculation as above, assuming again the same mass for all stars (no boosting from the stochastic sampling of the IMF is considered). The Ly α luminosity emerging from Pop-III stars of mass 1000, 300, and 100 M_{\odot} are $3.20 \times 10^{40}, 8.11 \times 10^{39},$ and 1.72×10^{39} erg s $^{-1}$. Under the assumption that $N(\text{Ly}\alpha) = N(M_{\text{UV}})$ (being Ly α and M_{UV} referring to the same star complex), the resulting T $_{\text{IGM}}(\text{Ly}\alpha)$ are 0.09, 0.11, and 0.16, respectively. These values double if the case-B is assumed, i.e., the predicted L(Ly α) is about a factor two fainter (Mas-Ribas et al. 2016). With such values of T $_{\text{IGM}}(\text{Ly}\alpha)$ the resulting EW $_0$ (Ly α) ranges between 4000-1500Å, for the three classes of Pop III stellar masses.

Future facilities are necessary to make a significant step forward. First, only the James Webb Space Telescope will access the optical rest-frame looking for the possible deficit of metals and the expected enormous Balmer emissions

(e.g., Inoue 2011), eventually gaining in depth with respect HST imaging. The next generation of Extremely Large Telescopes will also investigate the currently vague stellar component S by performing very deep imaging, while spectroscopy will address the deficiency of high-ionisation metal lines and the possible key HeII λ 1640 emission. The intrinsic HeII λ 1640/Ly α line ratio predicted for Pop III spans the range 0.01-0.10 (e.g., Schaerer 2013; Mas-Ribas et al. 2016), implying the expected flux of HeII λ 1640 would be $1.1 \times (10^{-21} - 10^{-20})/T_{\text{IGM}}(\text{Ly}\alpha)$ erg s $^{-1}$ cm $^{-2}$, clearly requiring an ELT-like telescope or an 8-10m class telescope in the most optimistic cases (T $_{\text{IGM}}(\text{Ly}\alpha) \ll 1$).

ACKNOWLEDGMENTS

We thank the anonymous referee for a constructive report. We thank Ll. Mas-Ribas and D. Schaerer for very stimulating discussions. This work is supported by PRIN-MIUR 2017 WSCC32. We acknowledge funding from the INAF mainstream (1.05.01.86.31). KC and GBC acknowledge funding from the ERC through the award of the Consolidator Grant ID 681627-BUILDUP. This work was supported in part by the NSF grant: COLLABORATIVE RESEARCH: The Final Frontier: Spectroscopic Probes of Galaxies at the Epoch of Reionization (AST-1815458, AST-1810822). MG acknowledges funding through HST-HF2- 51409.

REFERENCES

- Bacon, R., Accardo, M., Adjali, L., et al. 2010, Proc. SPIE, 7735, 773508
- Caminha, G. B., Grillo, C., Rosati, P., et al. 2017, A&A, 600, A90
- Dayal, P., & Ferrara, A. 2018, Phys. Rep., 780, 1
- Dijkstra, M., & Wyithe, J. S. B. 2007, MNRAS, 379, 1589
- Dijkstra, M. 2016, Understanding the Epoch of Cosmic Reionization: Challenges and Progress, 145
- Fan, X. 2012, Research in Astronomy and Astrophysics, 12, 865
- Hernán-Caballero, A., Pérez-González, P. G., Diego, J. M., et al. 2017, ApJ, 849, 82
- Inami, H., Bacon, R., Brinchmann, J., et al. 2017, A&A, 608, A2
- Inoue, A. K. 2011, MNRAS, 415, 2920
- Laursen, P., Sommer-Larsen, J., & Razoumov, A. O. 2011, ApJ, 728, 52
- Kashikawa, N., et al. 2012, ApJ, 761, 85
- Lotz, J. M., et al. 2017, ApJ, 837, 97
- Maseda, M. V., Bacon, R., Franx, M., et al. 2018, ApJ, 865, L1
- Mas-Ribas, L., Dijkstra, M., & Forero-Romero, J. E. 2016, ApJ, 833, 65
- Meneghetti, M., Rasia, E., Merten, J., et al. 2010, A&A, 514, A93
- Meneghetti, M., Natarajan, P., Coe, D., et al. 2017, MNRAS, 472, 3177
- Merlin, E., Pilo, S., Fontana, A., et al. 2019, A&A, 622, A169
- Neufeld, D. A. 1991, ApJ, 370, L85
- Plazas, A. A., Meneghetti, M., Maturi, M., et al. 2019, MNRAS, 482, 2823
- Rodney, S. A., et al. 2018, Nature Astronomy, 2, 324
- Salvaterra, R., Ferrara, A., & Dayal, P. 2011, MNRAS, 414, 847
- Schaerer, D. 2013, The First Galaxies, Astrophysics and Space Science Library, Volume 396, 345
- Shibuya, T., Ouchi, M., Harikane, Y., et al. 2018, PASJ, 70, S15
- Shimasaku, K., Kashikawa, N., Doi, M., et al. 2006, PASJ, 58, 313
- Sobral, D., Matthee, J., Darvish, B., et al. 2015, ApJ, 808, 139

- Sobral, D., Matthee, J., Brammer, G., et al. 2019, MNRAS, 482, 2422
- Steidel, C. C., Bogosavljević, M., Shapley, A. E., et al. 2011, ApJ, 736, 160
- Tornatore, L., Ferrara, A., & Schneider, R. 2007, MNRAS, 382, 945
- Vanzella, E., et al. 2017, MNRAS, 467, 4304
- Vanzella, E., et al. 2019, MNRAS, 483, 3618
- Visbal, E., Haiman, Z., & Bryan, G. L. 2016, MNRAS, 460, L59
- Wise, J. H. 2019, arXiv e-prints, arXiv:1907.06653
- Windhorst, R. A., et al. 2018, ApJS, 234, 41
- Zackrisson, E., González, J., Eriksson, S., et al. 2015, MNRAS, 449, 3057
- Zackrisson, E., & Vikaeus, A. 2019, arXiv e-prints, arXiv:1903.12555